



Universiteit
Leiden
The Netherlands

Photo-activated drug delivery systems

Kong, L.

Citation

Kong, L. (2018, June 7). *Photo-activated drug delivery systems*. Retrieved from <https://hdl.handle.net/1887/63080>

Version: Not Applicable (or Unknown)

License: [Licence agreement concerning inclusion of doctoral thesis in the Institutional Repository of the University of Leiden](#)

Downloaded from: <https://hdl.handle.net/1887/63080>

Note: To cite this publication please use the final published version (if applicable).

Cover Page



Universiteit Leiden



The following handle holds various files of this Leiden University dissertation:

<http://hdl.handle.net/1887/63080>

Author: Kong, L.

Title: Photo-activated drug delivery systems

Issue Date: 2018-06-07

5

Charge-Switchable Liposomes for Drug Delivery *in Vitro* and *in Vivo*

Abstract: Surface charge significantly affects how nanoparticles distribute *in vivo* as well as how they are taken up by cells. Herein, we report liposomal drug carriers whose surface charge can be rapidly switched *in situ* and *in vivo* using light. Prior to light activation, liposomes are neutrally charged and freely circulate within the bloodstream of an embryonic zebrafish following systemic (*i.v.*) administration. Upon light activation however, the liposome surface charge is rapidly switched from neutral to positively charged leading to rapid cellular adsorption and uptake. Switching of surface charge does not disrupt the integrity of the carrier membrane and small molecule cargos remain entrapped within liposomes and are taken up by cells.

Li Kong¹, Gabriela Arias Alpizar¹, Alexander Rabe², Michel Meijer¹, Sylvestre Bonnet¹, Stefan Vogel², Alexander Kros¹ and Fred Campbell¹

¹Leiden Institute of Chemistry, Leiden University, The Netherlands

²Department of Physics, Chemistry and Pharmacy, University of Southern Denmark, Odense, Denmark

5.1 Introduction

Nanoparticle-based approaches to target drugs to cancer cells have predominantly focused on long-circulating formulations designed to passively target tumors *via* the EPR effect. Doxil[®] and Myocet[®] are two liposomal-doxorubicin formulations clinically approved to treat a variety of human cancers in this way.^[1] Doxil[®] is a PEGylated liposomal formulation (ePC:Cholesterol:DSPE-mPEG₂₀₀₀;55:40:5) whereas Myocet[®] (POPC:Cholesterol:55:45) is non-PEGylated.^[2] Both formulations are 100-200nm in size and demonstrate extended circulation lifetimes (hours – days). The principle reason for this is reduced absorption of serum proteins (opsonisation) and avoidance of the MPS (*i.e.* recognition, uptake and clearance by plasma exposed macrophages, primarily in the liver and spleen). While Doxil[®] and Myocet[®] can efficiently accumulate within target tumors, their ability to evade cellular interactions *en route* to the tumor means they do not efficiently interact with target cancer cells. Drug delivery in these cases is achieved through passive diffusion of doxorubicin across the liposome membrane over time within the tumor.^[3] It is often therefore challenging to reach therapeutically relevant drug concentrations within tumors. In addition, given the fact that drug release occurs extracellular, these technologies are limited to the delivery of drugs which themselves can cross target cancer cell membranes. These technologies cannot easily be extended to the delivery of larger and/or more hydrophilic, membrane impermeable therapies (*e.g.* proteins and oligonucleotides).

In contrast, nanoparticles with a cationic surface charge are rapidly internalized by cells.^[4] This is caused by non-specific adsorption to anionic cell membranes (and/or the polyanionic glycocalyx) followed by endocytosis.^[5] In addition, it is thought that cationic nanoparticles can destabilize endosomal membranes facilitating endosomal escape and drug release to the cytosol of the cell.^[6] For these reasons, cationic nanoparticles have been extensively used as vehicles to deliver oligonucleotides (DNA and RNA) to cells *in vitro* (*e.g.* transfection agents such as Lipofectamine[®]).^[7] Here, they have the added advantage of efficiently condensing/complexing polyanionic genetic material. However the non-specific adsorption of cationic nanoparticles to cells, together with extensive adsorption of anionic serum proteins (opsonisation),^[8] has hampered the translation of these technologies *in vivo*. Efforts to sterically shield

nanoparticle cationic surface charge using PEG have been investigated,^[9] however unpublished work for our group has demonstrated this is an ineffectual method to prevent non-specific cellular interactions and therefore the rapid removal of nanoparticles from circulation (Figure S2). There are currently no cationic nanoparticle-based drug delivery systems approved for clinical use.

Previous work from our group utilized the embryonic zebrafish as a convenient animal model to assess the biodistribution of nanoparticles *in vivo*, at high (cellular) resolution and across a whole living organism.^[10] Here, it was found that the surface charge of liposomes significantly affects biodistribution. Notably, neutral liposomes based on the lipid composition of Myocet® were found to freely-circulate, whereas cationic liposomes, based on the lipid composition of EndoTAG-1^[11] – a positively charged liposomal-paclitaxel formulation currently in phase 3 clinical trials – were found to ‘stick’ across the entire endothelium of the fish (Figure S3). For a brief description of the embryonic zebrafish and its current applications in biomedical research, please see the supporting information.

Taking advantage of the contrasting biodistribution of differently charged liposomes *in vivo*, we here report an efficient strategy to convert freely circulating neutral liposomes to ‘sticky’ cationic liposomes *in situ* and *in vivo* using long-wave UV light as a trigger. We achieve this through the incorporation of neutrally charged, photocaged cholesterol analogues within liposome membranes. Upon light activation, photolysis of the photocage reveals a primary amine at the headgroup of cholesterol, which, protonated at physiological pH, results in a cationic liposome surface charge (Figure 1). In contrast to existing light activated liposomal drug delivery systems (DDS), a key feature of this system is not only surface charge switching but that this transformation does not lead to disruption of the liposome membrane and extracellular drug release. This technology provides the basis for the light targeted delivery of membrane impermeable cargos to target cells *in vivo*. A handful of similar strategies have been reported for micelle, polymersome and mesoporous silica based nanoparticle systems.^[12] All, however, rely on endogenous stimuli (both pH and enzymatic cleavage), with charge reversal occurring over the time frame of hours to days. These systems are therefore limited to applications where a) nanoparticles can

efficiently accumulate at the site of disease (e.g. tumor microenvironment) and b) there is an exploitable, pathological distinction between diseased and healthy tissue (e.g. low pH of tumor microenvironment).

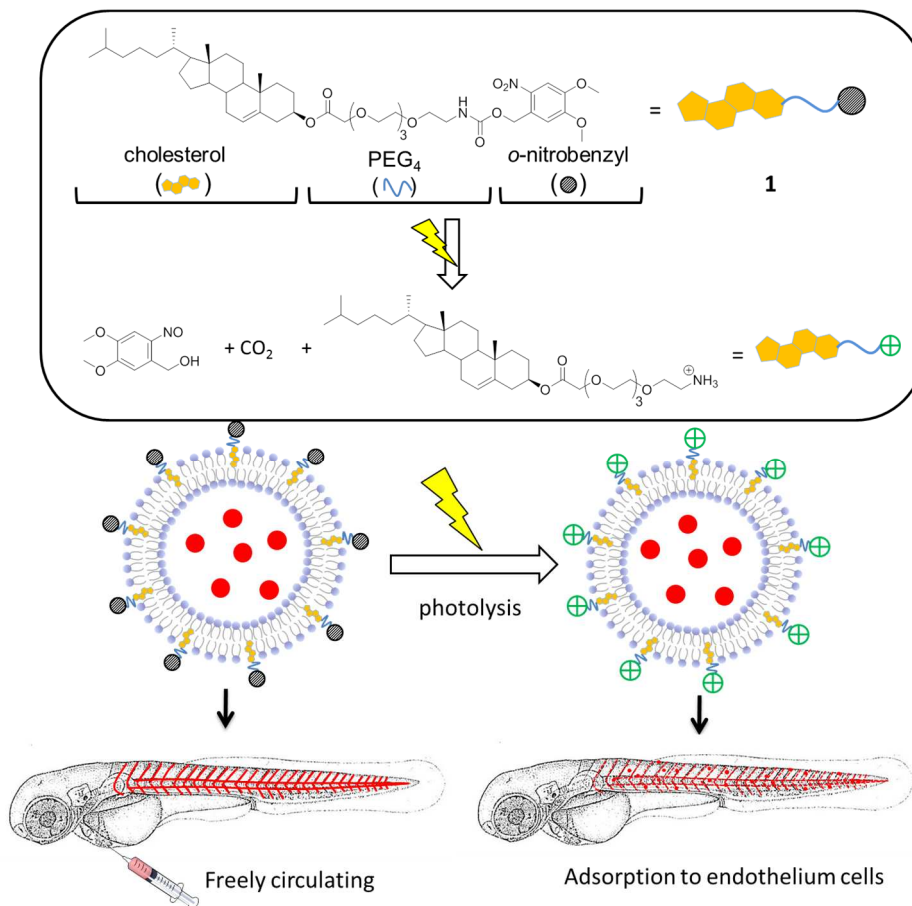
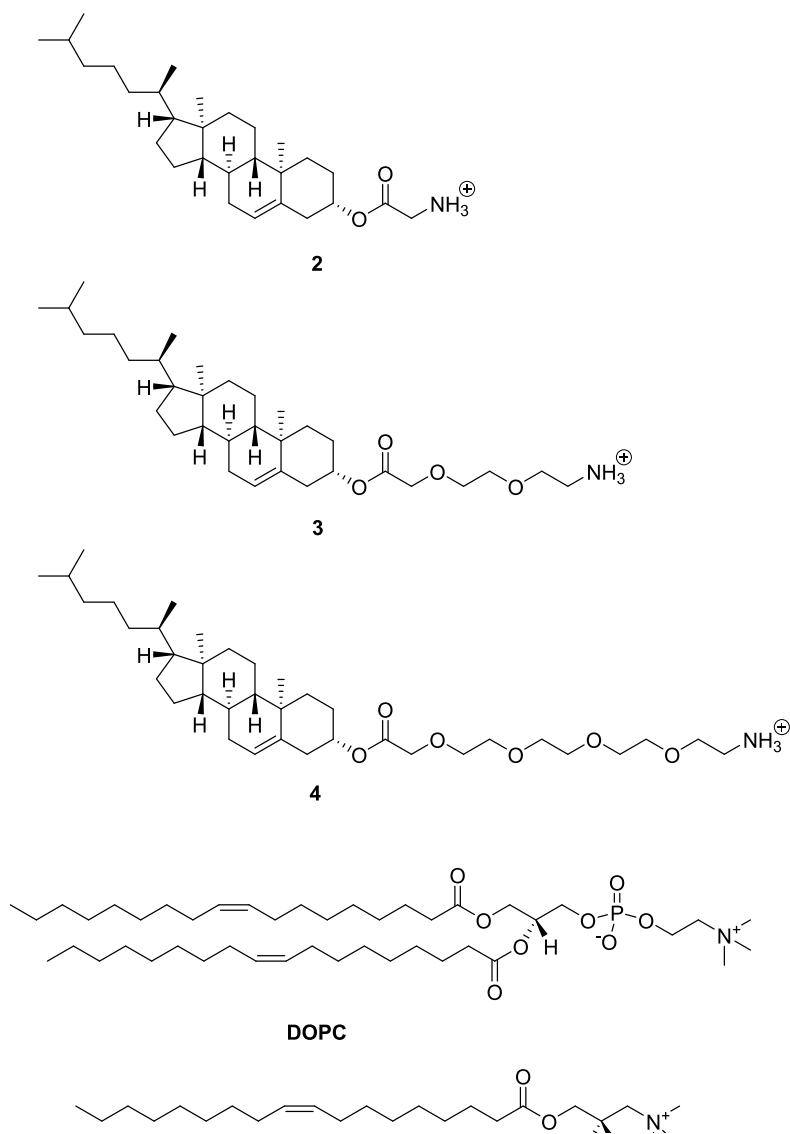


Figure 1. Schematic illustration of charge switchable liposome and its distribution *in vivo* before and after UV irradiation. The caged liposomes are freely circulating in the zebrafish prior to UV irradiation, while the cationic liposomes, triggered by UV light, stick to all endothelial cells and are endocytosed.

5.2 Results and discussion

To ensure sufficient cationic surface charge following photolysis of the *o*-nitrobenzyl photocage, a series of cationic lipids, based on cholesterol, were synthesized and tested. These lipids were co-formulated at 1:1 molar ratios with DOPC – to broadly match the lipid composition of Myocet[®]. As cholesterol is known to sit deeper within

phospholipid membranes – the hydroxyl headgroup being roughly in line with the phosphate group of adjacent phospholipids^[13] – a series of spacers, between cholesterol and primary amine, were designed to establish the optimal exposure of the terminal primary amine. Spacers chosen were glycine (**2**), PEG-2 (*i.e.* 2 ethylene glycol units; **3**) and PEG-4 (*i.e.* 4 ethylene glycol units; **4**), see Scheme 1.



Scheme 1. Structures of three cationic lipids with different spacers, DOPC and DOTAP.

From zeta potential measurements, it became clear that increasing the spacer length between cholesterol and terminal primary amine leads to a greater surface cationic charge (Figure 2a). In the case of DOPC:4 liposomes, a similar cationic surface charge was measured as compared to cationic liposomes formulated using the commercially available cationic lipid, DOTAP.^[14] As expected decreasing the mol% of these cationic lipids within the liposome formulation resulted in reduced overall cationic surface charge (Figure 2a).

Next, the biodistribution of liposomes containing each of these three cholesterol amine lipids mixed with DOPC (1:1 molar ratio) was assessed following intravenous (*i.v.*) injection in embryonic zebrafish. In all three cases, liposomes showed the expected non-specific adsorption across the entire endothelium of the embryonic fish (Figure 2b). From these experiments, it was decided that the cholesterol amine spacer with the longest (PEG₄) spacer would be taken forward, photocaged and assessed as a light activated drug delivery platform.

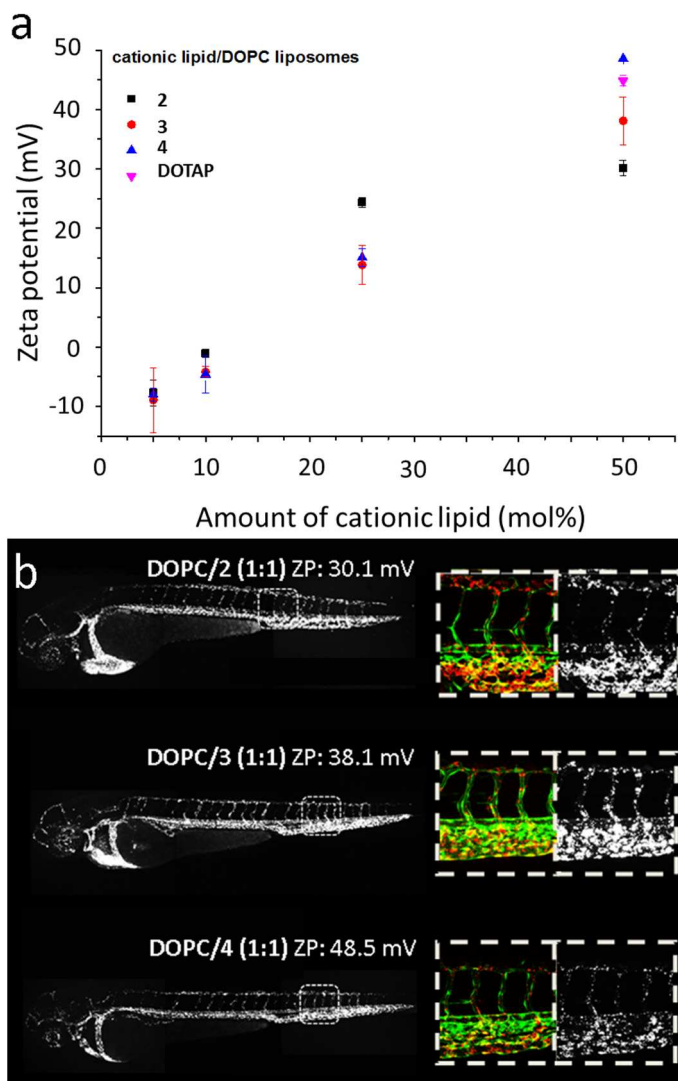


Figure 2. (a) Zeta potential of liposomes composed of mixtures of DOPC and cationic lipid: **2**, **3** or **4**. (b) Biodistribution of cationic liposomes containing 50 mol% of **2**, **3** or **4** injected (i.v.) in *kdrl:GFP* zebrafish embryos (2 days post fertilization, dpf). Embryos stably expressing GFP in all endothelial cells. Images acquired 1 hour post-injection (hpi). *Whole embryo images* (10x magnification): liposomes (white); *Boxed images* (40x magnification): left – blood vessels (green), liposomes (red); right: liposomes (white).

The synthesis and characterisation of photocaged, cholesterol amine (**1**) is described in the Supporting Information. A *o*-nitrobenzyl protection group was selected as a photocage for the amine given its ease of synthesis.^[15] Furthermore, it is well

characterized, neutral charged and has rapid photolysis kinetics, and can therefore be used in numerous biological scenarios. Upon UV light irradiation (365 nm, 15-17 mW/cm²) of **1** in H₂O:MeCN:^tBuOH (1:1:1), complete photolysis of the *o*-Nb functionality was achieved within 2 min (see Figure 3a and 3b). The appearance of three clear isosbestic points (295 nm and 365 nm) shows clean photoconversion of **1** to its photoproducts. To confirm that photolysis resulted in the generation of **4** with concomitant switching of liposome surface charge, zeta potential measurements of DOPC:**1** (1:1 mol ratio) liposomes were taken during photolysis (Figure 3c). This revealed a rapid switching of surface charge, from slightly anionic (-10 mV) to strongly cationic (+25 mV), within 2 min irradiation time. As expected, irradiation of control liposomes (100% DOPC) had no effect on surface charge. We are not currently able to explain the differences in zeta potential between DOPC:**4** liposomes formed following complete photolysis of **1** at the liposome surface (+25 mV) and those formulated directly as DOPC:**4** (+45 mV) liposomes. Importantly, light triggered charge switching of the liposome surface did not lead to apparent destabilization of the liposome membrane^[16] with liposome size and population polydispersity remaining constant before and after UV irradiation (Figure 3d). Caged, neutral liposomes (DOPC:**1**; 1:1) were stable for at least 2 days at 37 °C in biologically relevant solutions (buffer + serum) while kept in the dark, as the size of liposomes and corresponding polydispersity (PDI) barely changed over the time (Figure S9).

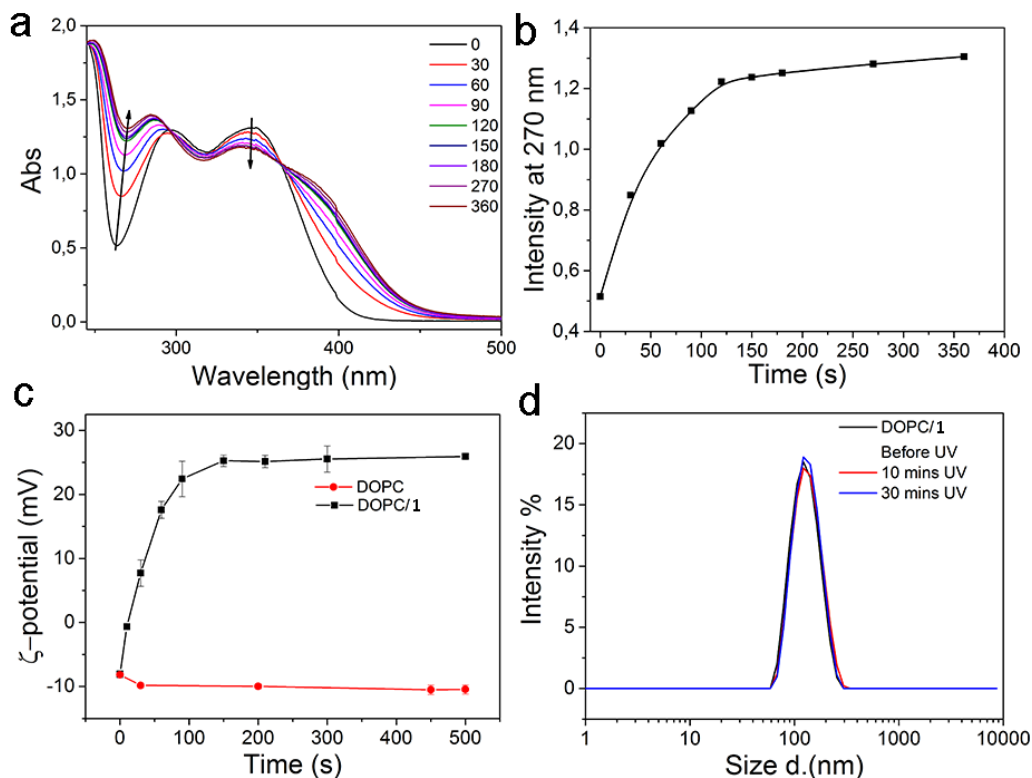


Figure 3. (a) Time evolution of the UV-VIS spectrum of **1** (100 μ M; H₂O:MeCN:^tBuOH (1:1:1)) during UV irradiation (365 nm, 15-17 mW/cm²), time points in seconds; (b) Time evolution of the UV absorbance at 270 nm; (c) The zeta potential of caged liposomes (DOPC/**1** 1:1) and DOPC liposomes with prolonged UV irradiation time; (d) The size distributions of caged liposomes (DOPC/**1** 1:1) before and after UV.

To investigate the biodistribution of DOPC:**1** liposomes (containing 1 mol% fluorescent probe) before and after light activation, liposomes were injected (*i.v.*) into embryonic zebrafish (approximately 2 dpf) and whole embryo images taken using a confocal fluorescent microscope (Figure 4). Prior to light activation, liposomes were freely circulating – as evidenced by the homogenous distribution of liposome associated fluorescence across the whole embryo – and largely restricted to the vasculature of the fish. No significant liposome interactions with either endothelial and/or plasma-exposed macrophages were observed. Following UV irradiation (365 nm, 15-17 mW/cm², 20 min) of the fish, liposomes – within the same embryo – are now clearly seen adsorbed to endothelial cells and across the entire vasculature of the fish. Photocaged liposomes in controls where animals were not exposed to light,

and imaged at the same time points, remained freely circulating (data not shown). From this, we concluded that a) liposomes prior to light activation are freely circulating, b) efficient photolysis of lipid **1** can be achieved *in situ* and *in vivo* and c) charge switching of liposome surface charge lead to the rapid adsorption of liposomes to endothelial cells of the fish vasculature.

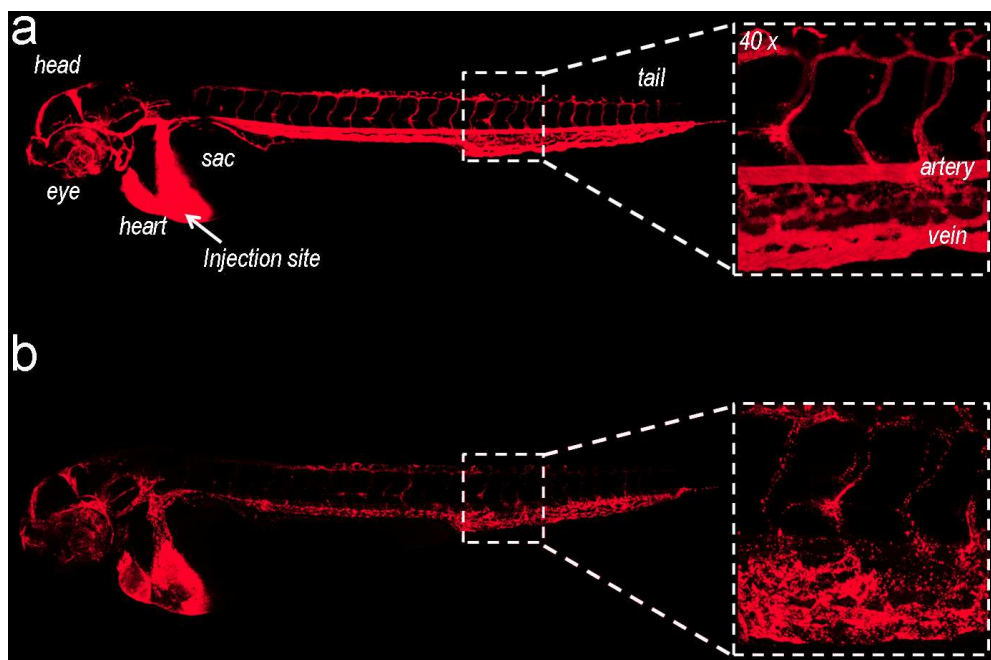


Figure 4. Biodistribution of caged liposomes (DOPC/**1** 1:1, containing 0.1% mol membrane dye; 1mM total lipids) in zebrafish embryos (2 dpf) before (a) and after (b) UV irradiation (365 nm, 15-17 mW/cm², 20 min). Images acquired 2 hpi, liposome-associated fluorescence in red. Injection (i.v.) volume: 1-2 nL.

For optimal application as a potential drug delivery system, we next investigated whether encapsulated contents remained entrapped within liposomes before, during and after UV irradiation. For this, we encapsulated a self-quenching concentration (10 mM) of the fluorescent dye sulforhodamine B (SR-B),^[17] and monitored the release (and associated fluorescence de-quenching) before and after UV irradiation (Figure 5a). From this data, it is clear that the dye remains encapsulated upon charge switching of the liposome membrane. Likewise, UV irradiation of control DOPC liposomes with encapsulated SR-B, which are insensitive to light activation, showed

also no dye release as expected. This confirmed that UV light does not itself physically compromise the integrity of liposome membranes. Transmission electron microscopy (TEM) imaging of SR-B encapsulated within DOPC:1 liposomes confirmed the presence of electron-rich (*i.e.* high contrast) SR-B within the core of the liposome before and after UV irradiation (Figure 5b and 5c). Importantly, these images also show the preservation of liposome morphology following charge switching of the liposome membrane.

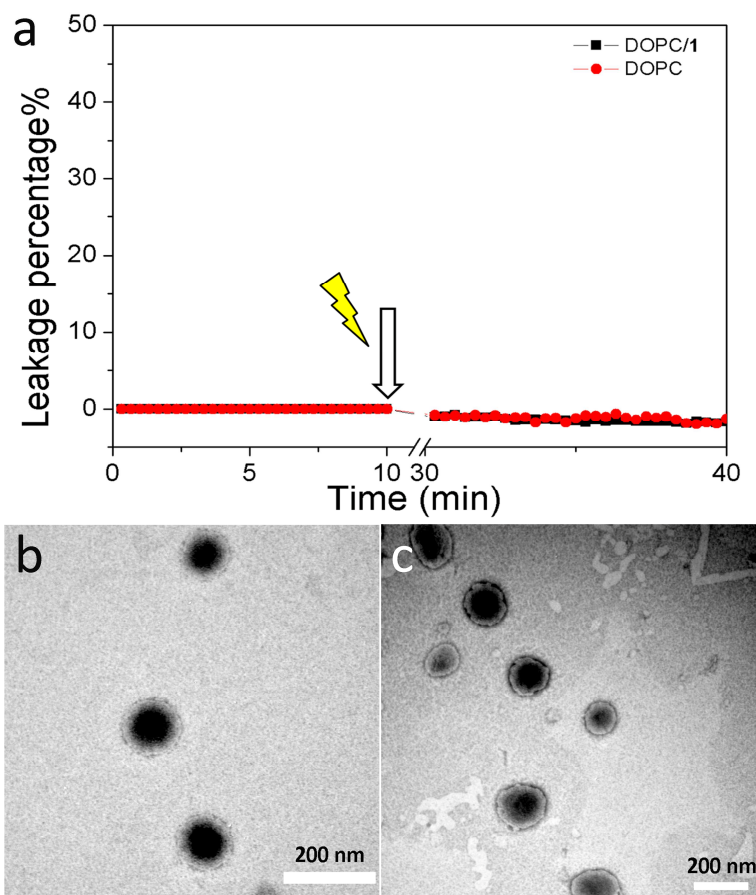


Figure 5. (a) Content leakage test on caged liposomes (DOPC/1 1:1) and DOPC liposomes containing sulforhodamine B (10 mM) with UV irradiation (365 nm, 15-17 mW/cm²). Arrow indicates the point at which samples were UV irradiated for 20 min. The observed minor drop in fluorescence can be attributed to UV irradiation induced photo bleaching. TEM images of caged liposomes containing SR-B (10 mM) prior to (b) and after (c) UV irradiation (365 nm, 15-17 mW/cm², 20 min).

Having established the successful light activated switching of liposome surface charge and drug encapsulation, we next investigated the potential for light triggered drug delivery to cells *in vitro*. Again using encapsulated self-quenching concentrations of SR-B, DOPC:1 liposomes were incubated with HeLa cells and imaged before and after 10 min UV irradiation (Figure 6). Prior to light activation, no delivery of SR-B to cells was observed, however following UV activation, increasing concentration of SR-B in the cells could be seen over time. The release of SR-B into the cell cytosol (and consequent de-quenching of fluorescence) requires active uptake of liposomes and subsequent endosomal escape. This accounts for the time delay between, presumably near instantaneous, liposome-cell membrane interactions following light activation and the visualization of released dye within the cell. These experiments confirm that liposomes are efficiently taken up by cells following light activation and surface charge switching, and that this leads to the successful intracellular delivery of membrane impermeable cargos to the cytosol of cells.

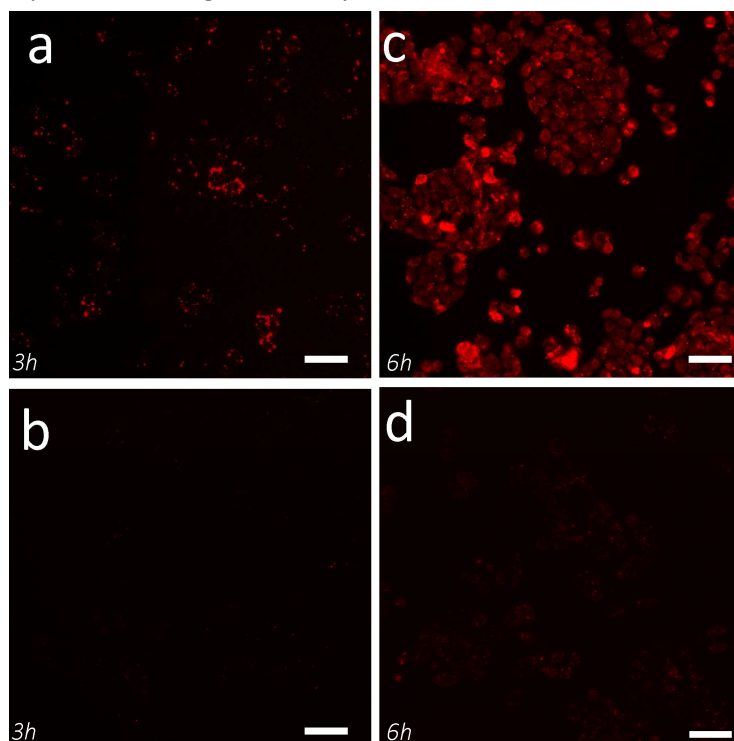


Figure 6. Fluorescent images of the cellular uptake of caged liposomes containing SR-B (10 mM), at 3 and 6 h post incubation, following (a,c) and without (b,d) UV irradiation. The scale bar represents 200 μm .

Finally, we assessed light triggered drug delivery via charge switching of liposome membranes *in vivo*. For this, we encapsulated propidium iodide (PI, 15 mM), a cell impermeable nuclear stain, within fluorescent (DOPE-Atto633, 0.5 mol%) photocaged liposomes composed of DOPC:1 (1:1 molar ratio). These liposomes were injected into a 2 dpf zebrafish embryo and imaged before and after irradiation *in situ* (365 nm, 15-17 mW/cm², 20 min). Without UV irradiation, caged liposomes freely circulated within the blood vessels of the embryonic fish (Figure 7a, blue). Following irradiation however, immobile liposomes can now be clearly seen absorbed across the entire vascular endothelium of the fish, appearing as distinct fluorescent punctae (Figure 7b, blue). Crucially, delivery of encapsulated PI, primarily to endothelial cells, is significantly enhanced following light activation and photoswitching of liposome surface charge (Figure 7, red). Endothelial cells are long and thin and PI associated fluorescence therefore appears to delineate the blood vessel lining. The larger and brighter fluorescent cells containing PI are plasma-exposed macrophages. Low level uptake of caged liposomes by these cells is observed in the absence of light activation (Figure 7a, white arrows). This data confirms that liposomes not only adsorb to cells following light activation but are taken up and are able to release the encapsulated cargos over time. This paves the way for light directed delivery of membrane impermeable therapeutic cargos *in vivo*.

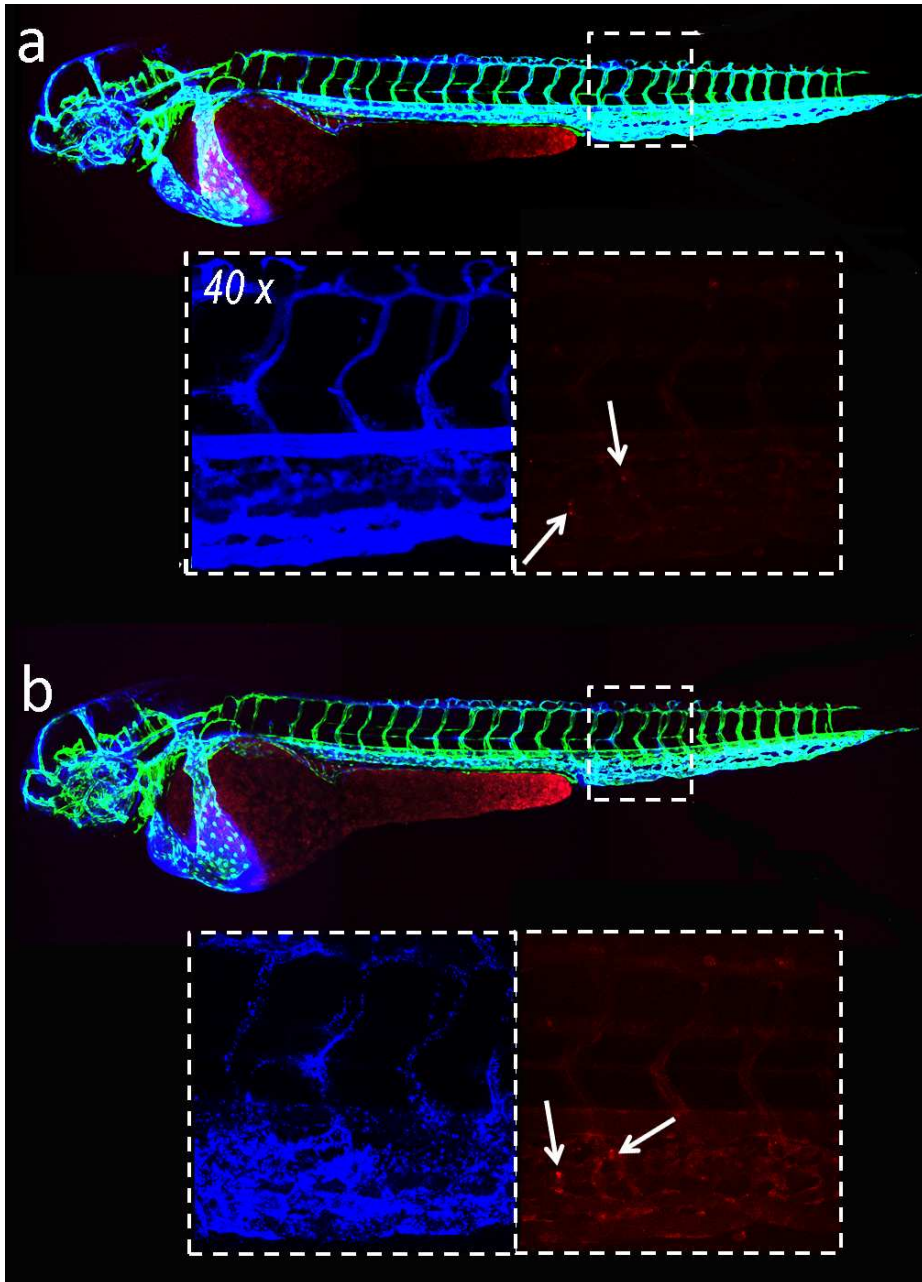


Figure 7. The distribution and cellular uptake of caged liposomes (DOPC/1 1:1 + 0.1% mol DOPE-ATTO633; 4 mM total lipids) containing 15 mM encapsulated PI in *kdrl:GFP* zebrafish embryos (2dpf) - before (a) and after (b) UV irradiation (365 nm, 15-17 mW/cm², 10 min). Injection volume: 1-2 nL. Images acquired 2 hpi. Blood vessels (green), liposomes (blue), PI (red).

5.3 Conclusions

In this work, we demonstrated successful switching of liposome surface charge *in situ* and *in vivo* using light as a trigger for activation. Prior to light activation, photocaged liposomes showed no interaction with cells *in vitro* and *in vivo* (following *i.v.* injection in embryonic zebrafish) and were freely circulating. Upon the light activation, the liposome surface charge switched rapidly to become cationic and as a result the liposomes adhered to, and were taken up by endothelial cells across the entire vasculature of the embryonic fish. Importantly, the encapsulated content was retained within the liposome before and after light activation. In this way, we were able to successfully demonstrate light targeted drug delivery of membrane impermeable cargos to cells *in vivo*. Compared to existing technologies, this approach offers complete (user defined) spatiotemporal control over drug delivery *in vivo* as well as the potential to deliver non-drug like and membrane impermeable therapies (*e.g.* proteins and oligonucleotides). It is important to note that light is used currently used in clinical application (*e.g.* during photodynamic therapy) and the maximal tolerable light dose (MTD) in humans is 1500–3700 J.^[18] In our experiments, embryonic zebrafish are subjected to a light dose of 4.85 J/cm² (145.5 mJ for the whole fish), several orders of magnitude below the MTD limit. In any event, the potential phototoxicity could be alleviated by using 2-photon excitation sources to obtain better tissue penetration with less harm to normal tissues.^[19]

5.4 Experimental

5.4.1 Materials and Instruments

1,2-dioleoyl-sn-glycero-3-phosphocholine (**DOPC**), 1,2-dioleoyl-3-trimethylammonium-propane (chloride salt) (**DOTAP**) and 1,2-dioleoyl-sn-glycero-3-phosphoethanolamine-N-(lissamine rhodamine B sulfonyl) (ammonium salt) (**DOPE-LR**) were purchased from Avanti Polar Lipids. 1,2-dioleoyl-sn-glycero-3-phosphoethanolamine-ATTO633 dye (**DOPE-ATTO633**) was purchased from ATTO-TEC GmbH. Cholesterol and all other chemical reagents were purchased at the highest grade available from Sigma Aldrich and used without further purification. All solvents were purchased from Biosolve Ltd. HEPES buffer: 10 mM HEPES, NaOH, pH 7.4. Phosphate buffered saline (PBS): 5 mM KH_2PO_4 , 15 mM K_2HPO_4 , 150 mM NaCl, pH 7.4. Sulforhodamine B solution (10 mM, pH=7.4) and propidium iodide (15 mM, pH=7.4) were prepared in PBS buffer. Silica gel column chromatography was performed using silica gel grade 40-63 μm (Merck). TLC analysis was performed using aluminium-backed silica gel TLC plates (60F 254, Merck), visualisation by UV absorption at 254 nm and/or staining with KMnO_4 solution. NMR spectra (^1H) were measured on a Bruker AV-400MHz spectrometer. Chemical shifts are recorded in ppm. Tetramethylsilane (TMS) is used as an internal standard. Coupling constants are given in Hz. Size exclusion chromatography was carried out using illustraTM NAPTM SephadexTM G-25 DNA grade pre-made columns (GE Healthcare) and used according to the user instructions.

Particle size distributions were obtained using a Malvern Zetasizer Nano ZS equipped with a peltier controlled thermostatic holder. The laser wavelength was 633 nm and the scattering angle was 173° . To obtain an estimation of the hydrodynamic radius, D_h , the Stokes-Einstein relation was used:

$$D = \frac{\kappa_B T}{3\pi\eta D_h}$$

where, k_B is the Boltzmann constant and η is the viscosity of the solvent. DLS measurements were carried out at room temperature.

UV irradiation was performed using a high-power LED (365 nm, 15-17 mW/cm², Roithner Laser Technik GmbH, Vienna, Austria) mounted at a fixed distance of 1 cm above the samples.

Fluorescence measurements for content leakage of liposomes were performed on a TECAN Plate Reader Infinite M1000. All experiments were carried out in 96-well plates (PP Microplate, 96 well, solid F-bottom (flat), chimney well). For every well the final volume was 200 µL. Fluorescent measurements were recorded at 25 °C.

The structure of the liposomes containing sulforhodamine B (SR-B) was characterized using transmission electron microscopy (TEM) operated at 70 kV (JEOL 1010, USA). a droplet of the sample was placed on a copper grid coated with a carbon film for 3 minutes and washed 3 times with water. Next the sample was stained with 0.5% uranyl acetate.

Zeta potentials were measured on a Zetasizer Nano ZS (Malvern) equipped with a dip-cell electrode. All samples (in 10 mM HEPES) were measured three times and at room temperature.

Size exclusion chromatography (SEC) was carried out using illustra™ NAP™ Sephadex™ G-25 DNA grade pre-made columns (GE Healthcare) and used according to the user instructions.

HeLa cells were cultivated in Dulbecco's Modified Eagle's Medium (DMEM), supplemented with 10% fetal calf serum (iron supplied), 2% L-glutamine, 1% penicillin and 1% streptomycin. Cells were cultured in an atmosphere of 5% CO₂ at 37°C. Medium was refreshed every two days and cells passaged at 70% confluence by treatment with trypsin-EDTA (0.05% trypsin).

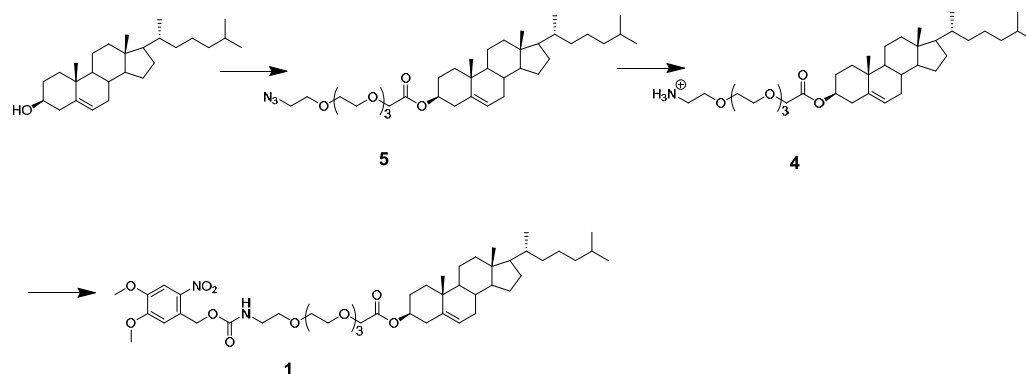
Fluorescence microscopy imaging of cells was done using an Olympus IX81 fluorescence microscope equipped with a filter cube (wavelength settings for SR-B Ex/Em: 565/586 nm).

Fluorescent images of zebrafish were acquired on Leica TCS SP8 confocal laser scanning microscope. Leica application suite advanced fluorescence software (LAS AF, Leica Microsystems B.V., Rijswijk, The Netherlands) and ImageJ (developed by the

National Institutes of Health) were used for image analysis and liposome colocalization studies. Wavelength settings for GFP Ex/Em: 485/530 nm (Ex laser: 488 nm), for propidium iodide Ex/Em: 535/617 nm (Ex laser: 543 nm), for NBD Ex/Em: 455/530 nm (Ex laser: 488 nm) and for ATTO 633 Ex/Em: 635/653 nm (Ex laser: 635 nm).

5.4.2 Synthesis of **1**

Photo-active lipid **1** was synthesized according to the following scheme.



Scheme 1. Synthesis scheme of photo-active lipid **1**.

Synthesis of **5**

Cholesterol (194 mg, 502 μmol , 1.00 eq.), 14-azido-3,6,9,12-tetraoxatetradecanoic acid (139 mg, 502 μmol , 1.00 eq.) and a catalytic amount of DMAP (6 mg, 50 μmol , 0.10 eq.) were dissolved in dry DCM (5 mL). A solution of EDC•HCl (192 mg, 1.00 mmol, 2.00 eq.) and DIPEA (0.13 mL, 753 μmol , 1.50 eq.) in dry DCM (5 mL) was added to the reaction mixture at 0 °C. The solution was stirred for 20 h at room temperature. DCM (40 mL) was added and the solution was washed with 1 M aqueous hydrochloric acid (2 x 50 mL) and a saturated aqueous sodium chloride solution (50 mL). The organic phase was dried over magnesium sulfate and the solvent was removed under reduced pressure. The crude product was purified by flash-column chromatography (petroleum ether (40–60 °C)/ethyl acetate 1:0 to 4:1 to 3:1 to 2:1) to obtain **5** (127 mg, 197 μmol , 39%) as a white solid. R_f = 0.37 (Pet. Ether: EtOAc; 1:1). $^1\text{H-NMR}$ (400 MHz, CDCl_3): δ (ppm) = 5.37 (s, 1H, C=CH), 4.80–4.60 (m, 1H, OCH_{chol}), 4.12 (s, 2H, CH_2COO), 3.78–3.60 (m, 14H, $\text{OCH}_2\text{CH}_2\text{O}$),

3.39 (d, $J = 2.2$ Hz, 2H, CH_2N_3), 2.33 (d, $J = 7.4$ Hz, 2H, $\text{CH}_2\text{C}=\text{CH}$), 2.07 – 0.80 (m, 38H, H_{chol}), 0.67 (s, 3H, CH_3CCH). **HR-MS** (ESI⁺): calc. ($\text{C}_{37}\text{H}_{63}\text{N}_3\text{O}_6\text{Na}$): $m/z = 668.46091$, found: $m/z = 668.46063$.

Synthesis of 4

5 (105 mg, 163 μmol , 1.00 eq.) was dissolved in dry THF (8 mL) and a solution of 1 M trimethylphosphine in toluene (0.49 mL, 489 μmol , 3.00 eq.) was added dropwise at 0 °C. The solution was warmed to room temperature and stirred for 3.5 h. A 1 M aqueous sodium hydroxide solution (25 mL) was added and the mixture was stirred for 1 h at room temperature. The solution was extracted with DCM (3 x 30 mL), the organic phase was washed with a saturated aqueous sodium chloride solution (30 mL) and dried over magnesium sulfate. The solvent was removed under reduced pressure. The crude product was purified by flash-column chromatography (DCM/MeOH 1:0 to 99:1 to 97:3 to 95:5 to 9:1, the eluent contained 1% of a 33% aqueous ammonia solution) to obtain **4** (37.4 mg, 60.2 μmol , 37%) as a white solid. $R_f = 0.21$ (CH_2Cl_2 :MeOH:aq. NH_3 (33%); 9:1:0.1). **¹H-NMR** (400 MHz, CDCl_3): δ (ppm) = 5.36 (d, $J = 3.9$ Hz, 1H, $\text{C}=\text{CH}$), 4.75 – 4.60 (m, 1H, OCH_{chol}), 4.10 (s, 2H, CH_2COO), 3.77 – 3.56 (m, 14H, $\text{OCH}_2\text{CH}_2\text{O}$), 3.50 (t, $J = 5.2$ Hz, 1H, $\text{CH}_2\text{CH}_2\text{NH}_2$), 2.85 (t, $J = 5.2$ Hz, 1H, $\text{CH}_2\text{CH}_2\text{NH}_2$), 2.31 (d, $J = 7.8$ Hz, 2H, $\text{CH}_2\text{C}=\text{CH}$), 2.07 – 0.83 (m, 38H, H_{chol}), 0.65 (s, 3H, CH_3CCH). **HR-MS** (ESI⁺): calc. ($\text{C}_{37}\text{H}_{66}\text{NO}_6$): $m/z = 620.48847$, found: $m/z = 620.48854$.

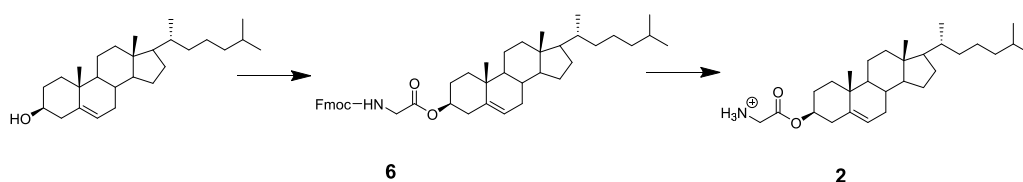
Synthesis of 1

The chloride salt of **4** (39.5 mg, 60.2 μmol , 1.00 eq.) and DIPEA (16 μL , 90.3 μmol , 1.50 eq.) were dissolved in DCM (3 mL). A solution of 4,5-Dimethoxy-2-nitrobenzyl chloroformate (33.2 mg, 120 μmol , 2.00 eq.) in DCM (3 mL) was added at 0 °C and the solution was stirred for 18 h at room temperature. DCM (10 mL) was added and the solution was washed with a 1 M aqueous hydrochloric acid solution (10 mL) and a saturated aqueous sodium chloride solution (10 mL). The organic phase was dried over magnesium sulfate and the solvent was removed under reduced pressure. The crude product was purified by flash-column chromatography (petroleum ether (40 – 60 °C)/ethyl acetate 1:0 to 3:1 to 1:1 to 1:3 to 0:1) to obtain **1** (10.6 mg, 12.3 μmol , 21%) as a colorless solid. $R_f = 0.18$ (Pet. Ether: EtOAc; 1:1). **¹H-NMR**

(300 MHz, CDCl₃): δ (ppm) = 7.72 (s, 1H, H_{Ar}), 7.07 (s, 1H, H_{Ar}), 5.70 – 5.58 (m, 1H, NH), 5.52 (s, 2H, CH₂,_{NVOC}), 5.43 – 5.26 (m, 1H, C=CH), 4.79 – 4.59 (m, 1H, OCH_{chol}), 4.11 (s, 2H, CH₂COO), 3.99 (s, 3H, OMe), 3.95 (s, 3H, OMe), 3.77 – 3.65 (m, 4H, OCH₂CH₂O), 3.60 (t, J = 4.9 Hz, 2H, NHCH₂CH₂), 3.44 (dt, J = 5.2, 4.8 Hz, 2H, NHCH₂), 2.32 (d, J = 7.3 Hz, 2H, CH₂C=CH), 2.09 – 0.83 (m, 38H, H_{chol}), 0.67 (s, 3H, CH₃CCH). **HR-MS** (ESI⁺): calc. (C₄₇H₇₄N₂O₁₂Na): m/z = 881.51340, found: m/z = 881.51353.

5.4.3 Synthesis of 2

Cationic lipid **2** was synthesized according to the following scheme.



Scheme S2. Synthesis scheme of cationic lipid **2**.

Synthesis of 6

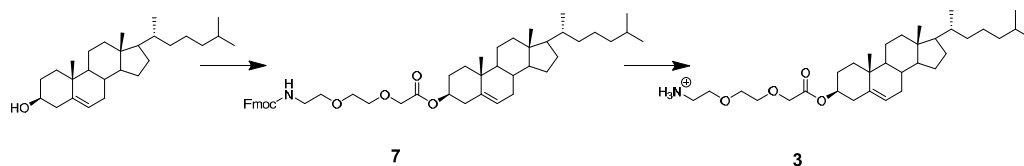
Cholesterol (500 mg, 1.29 mmol, 1.00 eq.), Fmoc-Gly-OH (577 mg, 1.94 mmol, 1.50 eq.) and EDC·HCl (744 mg, 3.88 mmol, 3.00 eq.) were dissolved in dry DCM (25 mL). A catalytic amount of DMAP (16 mg, 129 μ mol, 0.10 eq.) was added and the reaction mixture was stirred 24 h at room temperature. DCM (25 mL) was added and the solution was washed with a 1 M aqueous hydrochloric acid solution (2 x 50 mL), distilled water (50 mL) and a saturated aqueous sodium chloride solution (50 mL). The organic phase was dried over sodium sulfate and the solvent was removed under reduced pressure. The crude was purified by flash-column chromatography to obtain **6** (604 mg, 0.91 mmol, 70%) as a colorless solid. R_f = 0.34 (Pet. Ether(40 – 60 °C): EtOAc; 4:1). **¹H-NMR** (400 MHz, CDCl₃): δ (ppm) = 7.77 (d, J = 7.5 Hz, 2H, H_{Ar}), 7.61 (d, J = 7.5 Hz, 2H, H_{Ar}), 7.40 (t, J = 7.5 Hz, 2H, H_{Ar}), 7.32 (td, J = 7.5, 1.0 Hz, 2H, H_{Ar}), 5.38 (d, J = 4.0 Hz, 1H, C=CH), 5.29 (t, J = 5.4 Hz, 1H, NH), 4.77 – 4.63 (m, 1H, OCH_{chol}), 4.40 (d, J = 7.1 Hz, 2H, CH₂,_{Fmoc}), 4.24 (t, J = 7.1 Hz, 1H, CH_{Fmoc}), 3.98 (d, J = 5.4 Hz, 2H, CH₂NH), 2.34 (d, J = 7.8 Hz, 2H, CH₂C=CH), 2.09 – 1.04 (m, 26H, H_{chol}), 1.02 (s, 3H, CH₃CC=CH), 0.91 (d, J = 6.5 Hz, 3H, CH₃CHCH), 0.87 (d, J = 1.8 Hz, 3H, CH₃CHCH₃), 0.86 (d, J = 1.8 Hz, 3H, CH₃CHCH₃), 0.68 (s, 3H, CH₃CCH).

Synthesis of 2

6 (201 mg, 302 μmol) was dissolved in DCM/DEA (1:1, 4 mL) and stirred for 3 h at room temperature. The solvent was removed under reduced pressure and DEA residues were co-evaporated with methanol (3 x 10 mL). The crude was dissolved in DCM and purified by flash-column chromatography (DCM/MeOH 1:0 to 99:1 to 95:5) to obtain **2** (87.4 mg, 197 μmol , 65%) as a pale yellow solid. $R_f = 0.34$ (CH_2Cl_2 :MeOH; 9:1). $^1\text{H-NMR}$ (400 MHz, CDCl_3): δ (ppm) = 5.38 (d, $J = 3.7$ Hz, 1H, C=CH), 4.73 – 4.60 (m, 2H, NH_2), 3.41 (s, 2H, CH_2NH_2), 2.32 (d, $J = 7.9$ Hz, 2H, $\text{CH}_2\text{C}=\text{CH}$), 2.06 – 1.04 (m, 26H, H_{chol}), 1.01 (s, 3H, $\text{CH}_3\text{CC}=\text{CH}$), 0.91 (d, $J = 6.3$ Hz, 3H, CH_3CHCH), 0.87 (s, 3H, CH_3CHCH_3), 0.85 (s, 3H, CH_3CHCH_3), 0.67 (s, 3H, CH_3CCH).

5.4.4 Synthesis of 3

Cationic lipid **3** was synthesized according to the following scheme.



Scheme S3. Synthesis scheme of cationic lipid **3**.

Synthesis of 7

Cholesterol (100 mg, 259 μmol , 1.00 eq.), 2-(2-(Fmoc-amino)ethoxy)ethoxy]acetic acid (100 mg, 259 μmol , 1.00 eq.) and *cat.* amounts of DMAP (6.00 mg, 49.1 μmol , 0.20 eq.) were dissolved in dry DCM (2 mL). A solution of EDC-HCl (99.2 mg, 517 μmol , 2.00 eq.) and DIPEA (0.07 mL, 389 μmol , 1.50 eq.) in dry DCM (4 mL) was added dropwise to the reaction mixture at 0 $^\circ\text{C}$. The solution was allowed to warm up to room temperature and stirred for 18 h. The reaction mixture was diluted with DCM (20 mL), washed with 1 M aq. hydrochloric acid (2 x 30 mL), water (30 mL) and brine (30 mL). The organic phase was dried over magnesium sulfate and the solvent was removed under reduced pressure. The crude was purified by flash-column chromatography (petroleum ether (40 – 60 $^\circ\text{C}$)/ethyl acetate 1:0 to 4:1 to 2:1 to 1:1) to obtain **7** (125 mg, 166 μmol , 64%) as colorless solid. $R_f = 0.21$ (CH_2Cl_2 : MeOH; 17:3). $^1\text{H-NMR}$ (400 MHz, CDCl_3): δ (ppm) = 7.76 (d, $J = 7.5$ Hz, 2H, H_{Ar}), 7.62 (d, $J = 7.4$ Hz,

2H, H_{Ar}), 7.39 (t, $J = 7.5$ Hz, 2H, H_{Ar}), 7.31 (td, $J = 7.4, 0.9$ Hz, 2H, H_{Ar}), 5.52 (t, $J = 5.2$ Hz, 1H, NH), 5.32 (d, $J = 4.2$ Hz, 1H, C=CH), 4.77 – 4.66 (m, 1H, OCH_{chol}), 4.37 (d, $J = 7.2$ Hz, 2H, CH_{2, Fmoc}), 4.22 (t, $J = 7.2$ Hz, 1H, CH_{Fmoc}), 4.11 (s, 2H, CH₂COO), 3.78 – 3.64 (m, 4H, OCH₂CH₂O), 3.60 (t, $J = 5.1$ Hz, 2H, NHCH₂CH₂), 3.43 (q, $J = 5.1$ Hz, 2H, NHCH₂), 2.32 (d, $J = 7.9$ Hz, 2H, CH₂C=CH), 2.10 – 1.00 (m, 26H, H_{chol}), 0.98 (s, 3H, CH₃CC=CH), 0.91 (d, $J = 6.5$ Hz, 3H, CH₃CHCH), 0.88 (d, $J = 1.9$ Hz, 3H, CH₃CHCH₃), 0.86 (d, $J = 1.8$ Hz, 3H, CH₃CHCH₃), 0.66 (s, 3H, CH₃CCH).

Synthesis of **3**

7 (104 mg, 138 μ mol) was dissolved in DCM/DEA (1:1, 4 mL) and stirred for 3 h at room temperature. The solvent was removed under reduced pressure and DEA residues were co-evaporated with methanol (3 x 30 mL). The crude was dissolved in DCM and purified by flash-column chromatography (DCM/MeOH 1:0 to 9:1 to 17:3) to obtain **3** (28.4 mg, 53.4 μ mol, 39%) as a pale yellow solid. $R_f = 0.21$ (CH₂Cl₂:MeOH; 17:3). ¹H-NMR (400 MHz, CDCl₃): δ (ppm) = 6.86 (s_{br}, 2H, NH₂), 5.37 (s, 1H, C=CH), 4.77 – 4.53 (m, 1H, OCH_{chol}), 4.12 (s, 2H, CH₂COO), 3.85 (s, 2H, NH₂CH₂CH₂), 3.72 (s, 4H, OCH₂CH₂O), 3.26 (s, 2H, NH₂CH₂), 2.31 (d, $J = 7.6$ Hz, 2H, CH₂C=CH), 2.10 – 1.03 (m, 26H, H_{chol}), 1.00 (s, 3H, CH₃CC=CH), 0.90 (d, $J = 6.0$ Hz, 3H, CH₃CHCH), 0.86 (s, 3H, CH₃CHCH₃), 0.84 (s, 3H, CH₃CHCH₃), 0.66 (s, 3H, CH₃CCH).

5.4.5 Photolysis of **1**

The photolysis process of compound **1** was monitored by UV-VIS spectroscopy. A solution of **1** (100 μ M) in acetonitrile:tert-Butanol:water (1:1:1) was irradiated under a LED UV lamp (365 nm, 17 mW) at a fixed distance of 1 cm for 30 seconds and a UV spectrum scan was taken. UV absorption spectra were measured using a Cary 3 Bio UV-vis spectrometer, scanning from 200 nm to 550 nm at 1 nm intervals, scan rate: 120 nm/min. Next, the sample was irradiated for different time periods (60, 90, 120, 150, 180, 270 and 360 seconds) and spectra were measured.

5.4.6 Liposome preparation

Liposomes were prepared *via* extrusion using a mini-extruder (Mini-extruder, Avanti Polar Lipids, Alabaster, US). Lipid stock solutions in chloroform were prepared firstly with a total lipid concentration of 10 mM. For each sample, the relevant lipid film

including membrane dye (DOPE-ATTO633) was formed by evaporating organic solvents under N_2 , and hydrated for 20 min using HEPES buffer. The hydrated lipid film was vortexed for at least 1 min to obtain a suspension ([lipid]=10 mM with 0.5 mol% of DOPE-ATTO633). The solution was extruded 11 times through a 400 nm pore membrane to form multilayer vesicles (MLVs) at room temperature. Next the MLVs suspension was sequentially extruded 11 times through a 100 nm pore membrane to generate liposomes. The size distribution and PDI of prepared liposomes was determined by dynamic light scatter (DLS) spectroscopy.

For liposomes containing sulforhodamine B (SR-B) or propidium iodide (PI), the same method was applied, except the hydration buffer was HEPES containing sulforhodamine B (10 mM)/propidium iodide (15 mM). A sephadex G25 size exclusion column was used to remove unencapsulated dye.

5.4.7 Content leakage assay

For content leakage assays, the fluorescence emission of SR-B (10 mM, excitation: 520 nm, emission: 580 nm) encapsulated liposomes ([lipid]=10 mM) was measured prior to UV irradiation for 10 min. The sample was measured again after 20 min of UV irradiation.

5.4.8 *In vitro* cellular uptake

For the cellular uptake experiments, cells ($2 \times 10^5 \text{ mL}^{-1}$) were transferred to 48-well cell culture plates (500 μL , Greiner bio-one, Cellstar[®]) and cultured for 24 h. Cage or activated liposomes (500 μL , [lipid]=10 mM) solution were added to the cells and incubated for 3 or 6 h. Before imaging, the excess of liposomes was removed and the cells were washed three times with DMEM medium.

5.4.9 Zebrafish injection

Zebrafish (strain AB/TL, line Tg(kdrl:egfp)s843)^[20] were handled according to the guidelines from the Zebrafish Model Organism Database, the directives of the local animal welfare committee of Leiden University and the common Directive 2010/63/EU of the European Parliament and the Council. Fertilization was performed by natural spawning at the beginning of the light period and eggs were raised at 28.5

°C in egg water (60 µg/ml Instant Ocean sea salts). Liposome solutions were injected into zebrafish embryos (2 dpf) according to a modified microangiography protocol. The embryos were anesthetized in 0.01% tricaine and embedded in agarose gel (0.4%) containing tricaine. 1 nL volumes were calibrated and injected into the sinus venosus/duct of Cuvier. A small pyramidal space, in which the liposome solutions ([lipid]=4 mM) were injected, was created by penetrating the skin with the glassy injection needle and gently pulling it back. The experimental zebrafish was irradiated directly under a UV source (365 nm, 15-17 mW/cm², 10 min) at a distance of 3 cm and imaged again. Embryos were excluded from the experiments in case there was no backward translocation of venous erythrocytes or when the yolk ball was damaged, which would reduce the amount of liposomes in circulation.

5.4.10 Light actinometry

The optical power density of the LED light source used was determined using an integrating sphere setup. For this, the 365-nm LED (H2A1-365, Roithner Lasertechnik, Vienna, Austria), driven by a custom-built LED driver (I = 350 mA), was positioned precisely 5 cm above the 6.0 mm aperture of an integrating sphere (AvaSphere-30-IRRAD, Avantes, Apeldoorn, The Netherlands). This sphere was connected by an optical fibre (FC-UV600-2, Avantes) to a UV-Vis spectrometer (AvaSpec-ULS2048L StarLine CCD spectrometer, Avantes). The setup was calibrated using a NIST-traceable calibration light source (Avalight-HAL-CAL-ISP30, Avantes). The LED was switched on, and allowed to warm up for 1 min, before a spectrum was recorded. The obtained spectrum was integrated to obtain the total incident optical power density (in mW/cm²). Light dosages (in J) per zebrafish were obtained by multiplying the optical power density by the average surface area of a zebrafish (0.03 cm²), and the irradiation time (600 s).

5.5 References

- [1] (a) Y. Barenholz, *Journal of Controlled Release* **2012**, *160*, 117-134; (b) C. E. Swenson, W. R. Perkins, P. Roberts, A. S. Janoff, *Breast* **2001**, *10*, 1-7.
- [2] M. Marty, *Breast* **2001**, *10*, 28-33.
- [3] A. Gabizon, R. Isacson, E. Libson, B. Kaufman, B. Uziely, R. Catane, C. G. Bendor, E. Rabello, Y. Cass, T. Peretz, A. Sulkes, R. Chisin, Y. Barenholz, *Acta Oncol* **1994**, *33*, 779-786.
- [4] (a) J. H. Kang, W. Y. Jang, Y. T. Ko, *Pharm Res* **2017**, *34*, 704-717; (b) B. B. Christina R. Miller, Shannon D. McLean, Kathy A. McGovern, and David F. O'Brien, *Biochemistry* **1998**, *37*, 12875-12883.
- [5] M. Schmitt-Sody, S. Strieth, S. Krasnici, B. Sauer, B. Schulze, M. Teifel, U. Michaelis, K. Naujoks, M. Dellian, *Clin Cancer Res* **2003**, *9*, 2335-2341.
- [6] E. Blanco, H. Shen, M. Ferrari, *Nat Biotechnol* **2015**, *33*, 941-951.
- [7] F. Cardarelli, L. Digiacomo, C. Marchini, A. Amici, F. Salomone, G. Fiume, A. Rossetta, E. Gratton, D. Pozzi, G. Caracciolo, *Sci Rep-Uk* **2016**, *6*.25879-25887.
- [8] D. E. Owens, N. A. Peppas, *Int J Pharm* **2006**, *307*, 93-102.
- [9] (a) P. Yingyuad, M. Mevel, C. Prata, S. Furegati, C. Kontogiorgis, M. Thanou, A. D. Miller, *Bioconjug Chem* **2013**, *24*, 343-362; (b) C. L. Chan, R. N. Majzoub, R. S. Shirazi, K. K. Ewert, Y. J. Chen, K. S. Liang, C. R. Safinya, *Biomaterials* **2012**, *33*, 4928-4935; (c) T. Gjetting, R. I. Jolck, T. L. Andresen, *Adv Healthc Mater* **2014**, *3*, 1107-1118.
- [10] F. Campbell, F. L. Bos, S. Sieber, G. A. Alpizar, B. Koch, J. Huwyler, A. Kros, J. Bussmann, *ACS Nano*, **2018**, accepted. DOI: 10.1021/acsnano.7b06995
- [11] P. Metz, O. Gottschalk, M. Schmitt-Sody, S. Luedemann, M. Eichhorn, B. Schulze, H. Bohnenkamp, E. Guenzi, U. Michaelis, M. Funk, *Ann Rheum Dis* **2007**, *66*, 288-288.
- [12] (a) D. J. Lee, Y. T. Oh, E. S. Lee, *Int J Pharm* **2014**, *471*, 127-134; (b) S. Tang, Q. Meng, H. Sun, J. Su, Q. Yin, Z. Zhang, H. Yu, L. Chen, W. Gu, Y. Li, *Biomaterials* **2017**, *114*, 44-53; (c) J. S. Hersey, C. M. LaManna, H. Lusic, M. W. Grinstaff, *Chem Phys Lipids* **2016**, *196*, 52-60; (d) Q.

Han, W. Wang, X. Jia, Y. Qian, Q. Li, Z. Wang, W. Zhang, S. Yang, Y. Jia, Z. Hu, *ACS Appl Mater Interfaces* **2016**, *8*, 18658-18663.

[13] S. AmitKessel, NirBen-Tal, *Biophysical Journal* **2001**, *81*, 643–658.

[14] B. K. Kim, G. B. Hwang, Y. B. Seu, J. S. Choi, K. S. Jin, K. O. Doh, *Bba-Biomembranes* **2015**, *1848*, 1996-2001.

[15] S. H. C. A. Li Kong, Sylvestre Bonnet, Alexander Kros and Frederick Campbell, *Angew. Chem. Int. Ed.* **2016**, *55*, 1396 –1400.

[16] S. J. Leung, M. Romanowski, *Theranostics* **2012**, *2*, 1020-1036.

[17] W. Bae, T. Y. Yoon, *Biophys J* **2013**, *104*, 88a-88a.

[18] S. K. P. Satish Krishnamurthy, Peggy Witmer and Tony Brown, *Lasers in Surgery and Medicine* **2000**, *27*, 224–234.

[19] K. Peng, I. Tomatsu, B. van den Broek, C. Cui, A. V. Korobko, J. van Noort, A. H. Meijer, H. P. Spaink, A. Kros, *Soft Matter* **2011**, *7*, 4881.

[20] L. D. Covassin, A. F. Siekmann, M. C. Kacergis, E. Laver, J. C. Moore, J. A. Villefranc, B. M. Weinstein, N. D. Lawson, *Dev Biol* **2009**, *329*, 212-226.

5.6 Supporting information

5.6.1 Zebrafish embryo, a Developmental Model Organism

Zebrafish are vertebrates which have been widely used in the scientific study of embryo development and gene function.^[1] Zebrafish embryos develop rapidly outside of the mother with all major organs, such as heart, brain and intestine, functionally developed by 36 hours post fertilization (hpf). By 36 hpf, zebrafish embryos have a closed circulatory system whose vasculature develops in anatomical form (Figure S1).

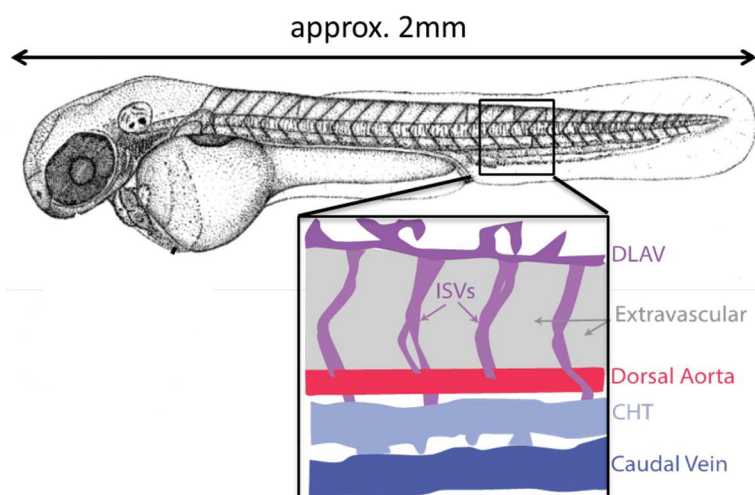


Figure S1 The caudal vascular system of zebrafish in the larval stage. The dorsal longitudinal anastomotic vessel (DLAV), the intersegmental vessels (ISVs), the extravascular tissue, the dorsal aorta, the caudal hematopoietic tissue (CHT) and the caudal vein are indicated.

There are various advantages of using zebrafish as a model organism system in scientific research. 1) The genome of zebrafish has fully sequenced and 70% homologous to humans. In the case of genes encoding disease-causing human proteins, this number increases to 82%. There have been numerous models of human diseases established in zebrafish.^[2] 2) Zebrafish are highly fecund, produce large clutches (100-200 embryos) and embryonic development is rapid and external of the mother. Testing can be carried out on large sample sets of animals and the cost of raising and maintaining zebrafish is much lower than that of mammals. 3) Zebrafish embryos are small and transparent allowing the *in vivo* observation of internal development and function, over the entire organism, using simple microscopy setups. The utility of zebrafish has been significantly enhanced by the generation of tissue-specific fluorescent transgenic zebrafish.

As a vertebrate model, zebrafish have wide biological applications, such as gene mapping, genome mutagenesis, transgenesis, chimeric embryo analysis, protein overexpression or

knockdown and chemical screens.^[3] Zebrafish mutant phenotypes, identified in forward genetic screens, have provided valuable insight into corresponding human disease pathophysiology.^[4] Likewise high-throughput chemical screens have proved invaluable as pre-clinical toxicological tests prior to initial screening in rodent models.^[5]

5.6.2 Additional figures

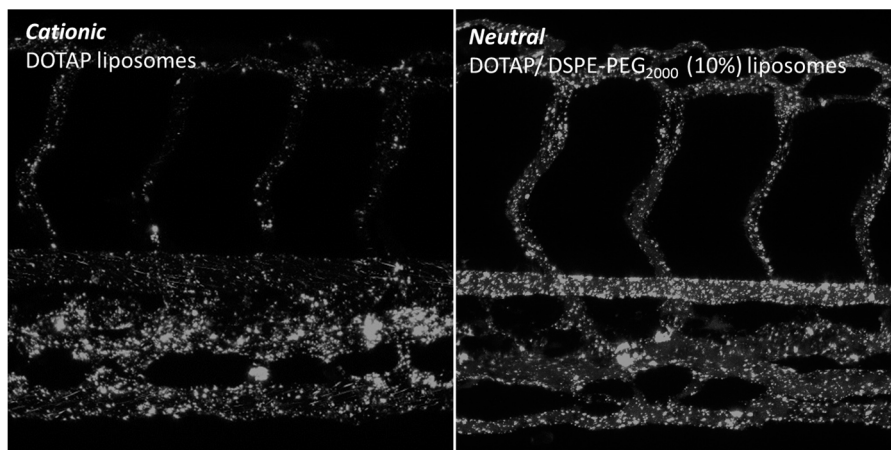


Figure S2. The distribution of cationic liposomes (DOTAP) and PEGylated cationic liposomes (DOTAP/DSPE-PEG₂₀₀₀; 9:1) within a zebrafish embryo. Fluorescently labeled liposomes ([lipid]= 1 mM, containing 1 mol% Rhod-PE) were injected into the duct of Cuvier of the embryonic fish at 54 hpf. Confocal microscopy was performed in a defined region caudal to the yolk extension at 1hpi. Image taken from unpublished data.

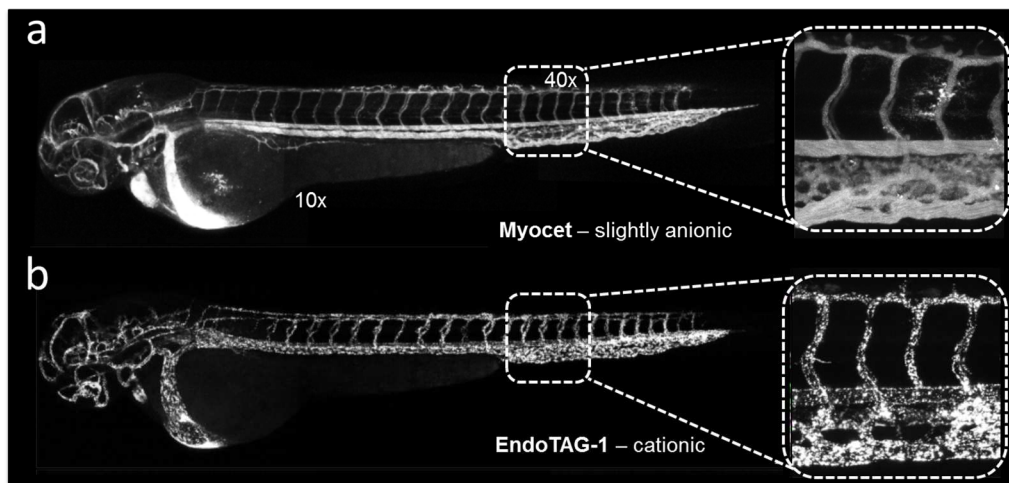


Figure S3. The distribution of neutral liposomes (Myocet) and cationic liposomes (EndoTAG-1) in zebrafish embryo.

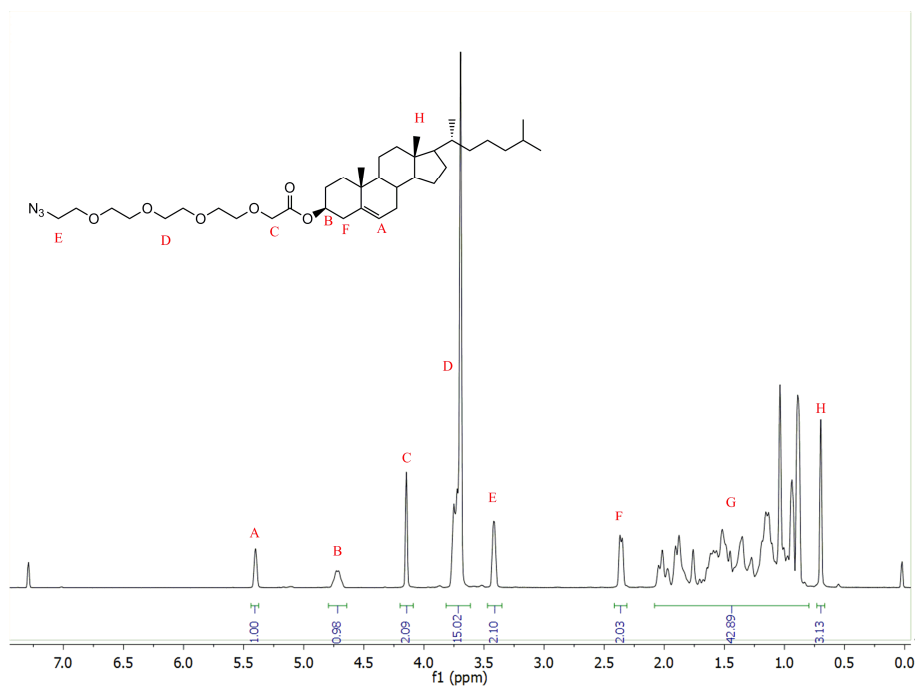


Figure S4. The $^1\text{H-NMR}$ structure of **5**.

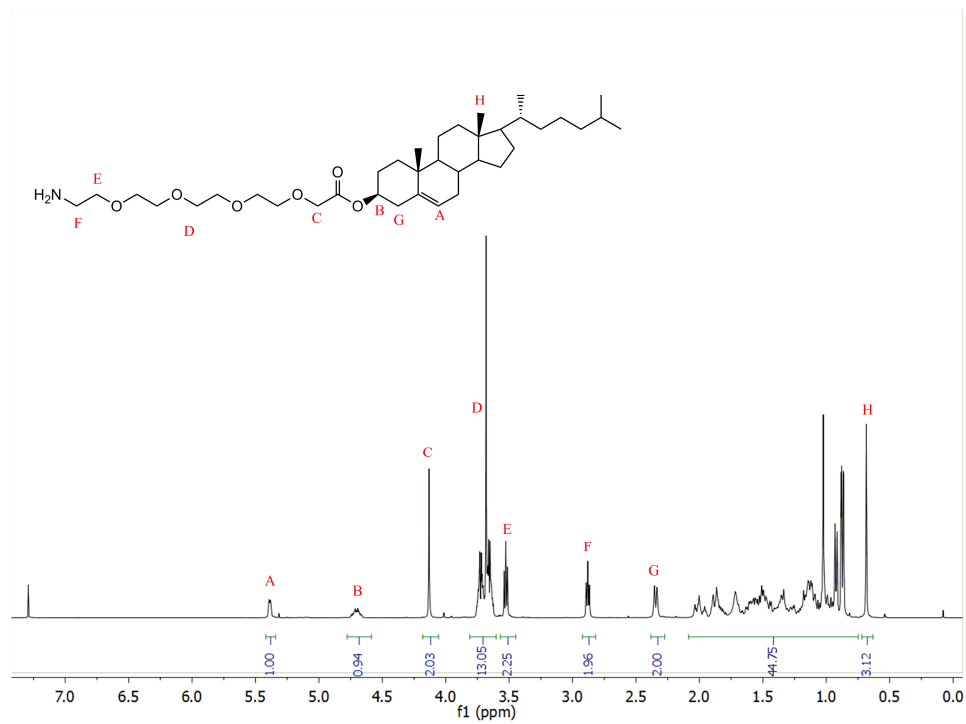


Figure S5. The ¹H-NMR structure of 4.

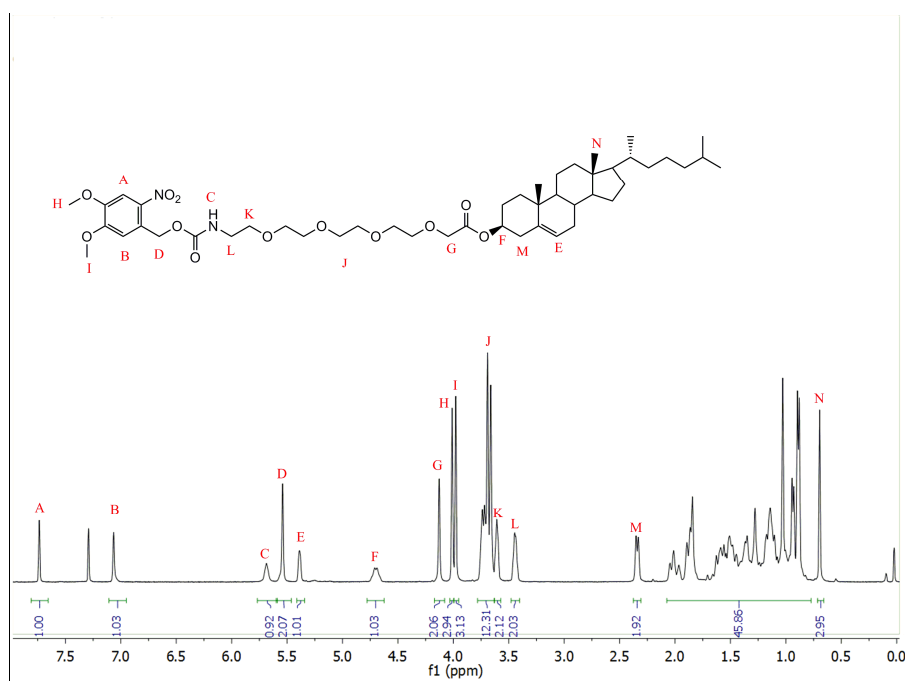


Figure S6. The ¹H-NMR structure of 1.

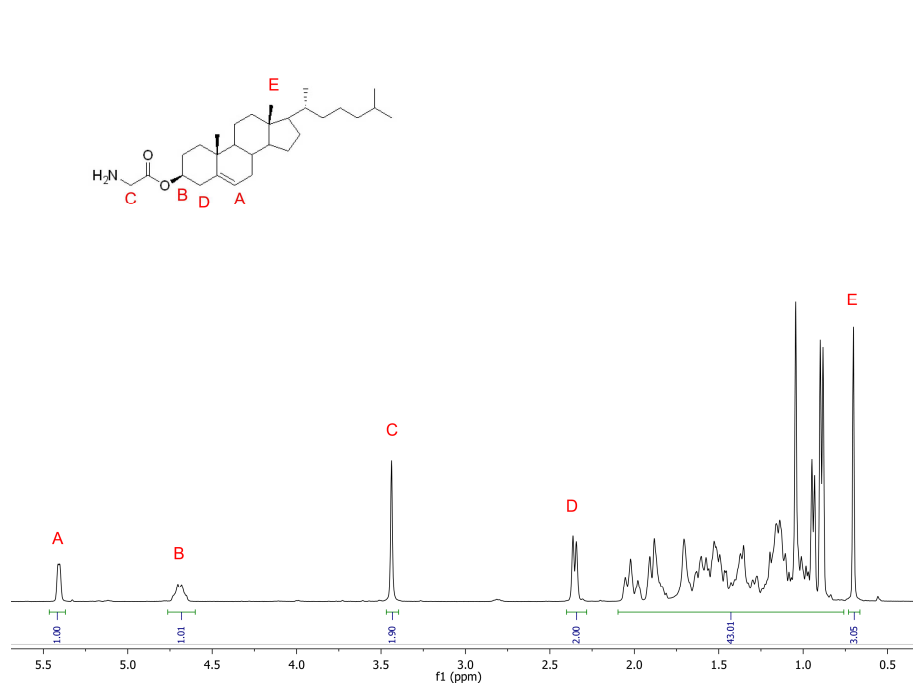


Figure S7. The $^1\text{H-NMR}$ structure of **2**.

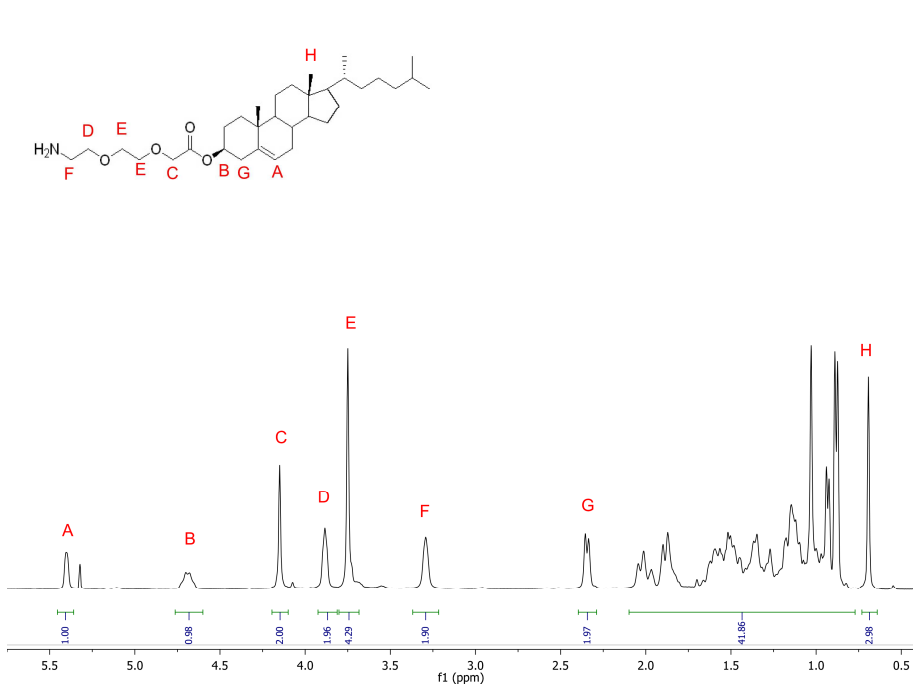


Figure S8. The $^1\text{H-NMR}$ structure of **3**.

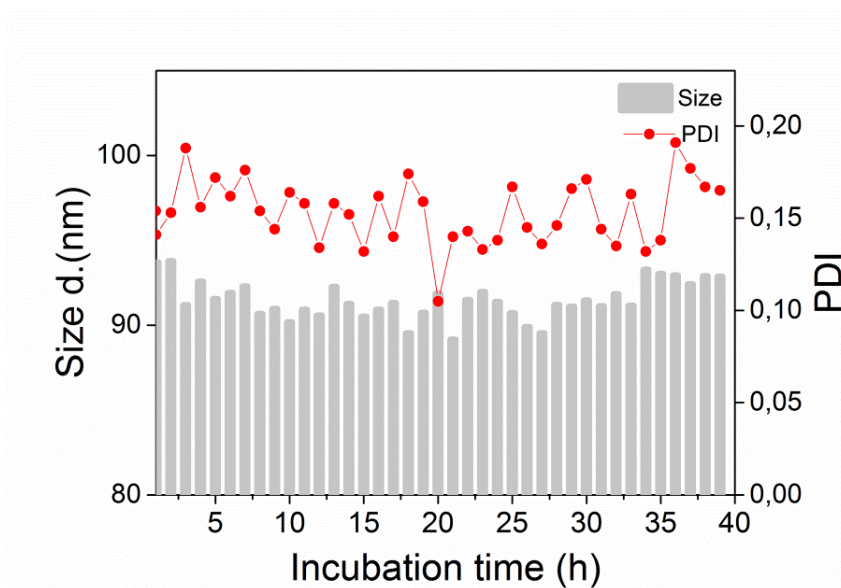


Figure S9. The size change and PDI of caged liposomes (DOPC/1 1:1) incubated with DMEM (+10% FCS) as a function of time.

References:

- [1] H. R. Zope, F. Versluis, A. Ordas, J. Voskuhl, H. P. Spaik, A. Kros., *Angew. Chem. Int. Ed.* **2013**, 52, 14247–14251.
- [2] A. F. Schier., *Nature*, **2013**, 496, 443–444.
- [3] G.N. Wheeler, A. W. Brandli, *Dev Dyn*, **2009**, 238,1287-1308.
- [4] G.J. Lieschke, P.D. Currie, *Nat Rev Genet*, **2007**, 8, 353-367.
- [5] (a) S. J. Poureetezadi, E. Donahue, R. A. Wingert, *J Vis Exp*, **2014**, 93, 5, 2063; (b) S. A. Brittijn, S. J. Duivesteijn, M. Belmamoune, L. F. M. Bertens, W. Bitter, J. D. De Bruijn, D. L. Champagne, E. Cuppen, G. Flik, C. M. R.A.J.Janssen, I.M.L.De Jong, E.R. De Kloet, A. Kros, A.H.Meijer, J. R. Metz, A. M. van der Sar, M. J.Schaaf,S. Schulte-Merker , H.P. Spaik, P. P Tak, F. J. Verbeek, M. J. Vervoordeldonk,F.J. Vonk, F. Witte, H. Yuan, M. K. RichardsonInt, *J Dev Biol.* **2009**, 53, 835-850.